#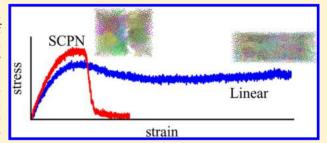 The Effect of Intrachain Cross-Linking on the Thermomechanical Behavior of Bulk Polymers Assembled Solely from Single Chain Polymer Nanoparticles

Suwon Bae,[†] Or Galant,[‡] Charles E. Diesendruck,[‡] and Meredith N. Silberstein*,[†]

[†]Sibley School of Mechanical and Aerospace Engineering, Cornell University, Ithaca, New York 14850, United States
[‡]Schulich Faculty of Chemistry and Russell-Berrie Nanotechnology Institute, Technion - Israel Institute of Technology, Haifa, Israel

S *Supporting Information*

ABSTRACT: Chemical cross-linking of polymer chains is a powerful means for tailoring the thermomechanical properties of bulk plastics. Nonetheless, upon cross-linking, processability is reduced as the plastic becomes thermoset. Here, molecular dynamics simulations are used to study the effects of intramolecular chemical cross-linking on chain topology and thermomechanical properties of a bulk, thermoplastic polymer. Polyethylene (PE)-like plastics are assembled purely from chains which have undergone a set level of intrachain cross-linking (to form single chain polymer nanoparticles, SCPNs). We have

analyzed the chain topology at an equilibrated state in terms of chain unfolding and entanglement by radius of gyration and primitive path, respectively. The extents of both chain unfolding and chain entanglement were found to decrease with increasing intrachain cross-linking ratio. By applying simulated cooling, uniaxial tension, and uniaxial compression, we characterized the thermomechanical properties at the glassy state. The simulated mechanical testing shows that the bulk polymer becomes stiffer, stronger, and more brittle as the intrachain cross-linking ratio is increased. We observe that the failure of the SCPN-based bulk polymers is a consequence of separation between SCPNs. This study successfully elucidates the effect of intramolecular cross-linking on the thermomechanical properties at bulk, as a clear correlation is shown between the amount of covalent intrachain collapse and interchain interactions.

1. INTRODUCTION

Polymers are materials composed of macromolecular chains, and their thermomechanical properties are determined by both intra- and interchain interactions. Because both interactions are associated with the underlying structure of a polymer, this structure is a powerful means of controlling the thermomechanical response of a polymer. Cross-linking between chains has been shown to change the internal structure and the thermomechanical properties of an otherwise linear glassy polymer. Small amounts of interchain cross-links, covalent or noncovalent, typically reduce the peak stress but enhance ductility while large amounts of interchain cross-links typically increase strength and decrease toughness.[1−5] Interchain cross-links change formability as well as the mechanical properties, preventing the polymer from being thermally processed or reprocessed. Intrachain cross-links also change the chain topology of a bulk polymer but unlike interchain cross-links keep the polymer still thermally processable.[6] In this molecular dynamics (MD) simulation study, we adopt intrachain cross-linking to produce a bulk polymer and investigate its effects on chain topology and thermomechanical properties.

The thermoplastic polymer architecture obtained via intrachain cross-linking is commonly known as single chain polymer nanoparticles (SCPNs). Individual SCPN structure

can be precisely controlled through the amount of chain functionalization in the linear precursor.[7] Intramolecular cross-linking (collapse) has emerged as a synthetic route to produce small polymer nanoparticles which could not be obtained from emulsion polymerization.[8,9] SCPN synthesis techniques have been growing sophisticated in recent years, and individual, independent SCPNs have been extensively studied in terms of shape, size, and chemistry.[10−13] In contrast, little research has been conducted on intrachain cross-linking in bulk polymers.[6,14] We have previously synthesized bulk polymers assembled from poly(methyl methacrylate) SCPNs and experimentally characterized their glass transition temperature and their behavior below the glass transition temperature.[14] We found that with increasing intrachain cross-linking ratio the material fails earlier, peak stress decreases, and the glass transition temperature of the bulk polymer increases, but that the elastic modulus does not change substantially. We have concluded from these findings that for glassy polymers the elastic response is not affected by intrachain cross-linking; however, the plastic response is affected.

A

The aim of this paper is to use MD simulations to further understand the effect of intrachain cross-linking on the thermomechanical behavior of bulk polymers assembled purely from SCPNs. MD is a facile approach for identifying relationships between molecular level structure and bulk properties. In particular, trajectories extracted from MD simulations allow us to take a closer look at the chain topology of the assembly of SCPNs than we can readily obtain from experiments. We develop MD models of bulk polymers assembled purely from SCPNs with three different cross-linking ratios and from linear chains for reference. Configurations are analyzed in terms of chain unfolding, chain entanglement, and segmental dynamics. The SCPN assembly thermomechanical properties are characterized by glass transition temperature and responses to uniaxial tension and compression.

2. METHODS

2.1. Molecular Dynamics Model. A polyethylene (PE)-like polymer with degree of polymerization of 1000 was chosen to represent individual SCPNs and linear chains. Every methylene group was coarse-grained into a single neutral bead. The interactions between beads were described by a modified DREIDING potential.[15,16] Each SCPN model was produced from a linear chain as detailed in our prior publication.[17] Briefly, the beads were randomly functionalized as potential cross-linking sites according to the target cross-linking ratio. The chains were then alternatively equilibrated and cross-linked following a distance-based criteria until the cross-linking ratio was within 0.5% of the target. We prepared three different MD models of SCPNs for each of three different cross-linking ratios (5%, 10%, and 15%) and five different initial configurations of each model. Each model is distinct and presents a unique distribution of cross-link sites.

To create the bulk materials, we then replicated and randomly located 27 nonoverlapping nominally identical SCPNs in a simulation box. This number of SCPNs was chosen based on convergence of the stress−strain behavior under tension (see Supporting Information Figure S2). Periodic boundary conditions were imposed in order for the response of the simulation box to be representative of bulk polymer behavior. The simulation box was then subjected to simulated annealing as detailed in Table 1. The simulated

Table 1. Procedure of Simulated Annealing for Assemblies of SCPNs[a]

	T_{start} [K]	T_{end} [K]	P_{start} [atm]	P_{end} [atm]	duration [ns]
1	500	500	10	10	10
2	500	150	10	10	25
3	150	150	10	10	10
4	150	150	10	0	25
5	150	150	0	0	25

[a]T and P stand for temperature and pressure, respectively.

annealing entailed holding at a high temperature and pressure, cooling under pressure, and then releasing the pressure. Temperature and pressure were controlled through each step, implemented by NPT dynamics with a Nosé−Hoover thermostat. The velocities and positions of the beads were updated each 1 fs by time integration utilizing the velocity-Verlet time stepping scheme. For each cross-linking ratio, three different MD models were prepared, each model originating

from an SCPN with a unique distribution of intrachain cross-links. All MD simulations were performed using the large scale atomic/molecular massively parallel simulator (LAMMPS)[18] and the Extreme Science and Engineering Discovery Environment (XSEDE) Stampede 2 cluster.[19]

2.2. Configurations at an Equilibrated State. The prepared MD models were analyzed in terms of configuration and segmental dynamics at an equilibrated state. The configurations were captured as snapshots using the VMD software package.[20]

The radii of gyration of the individual SCPNs composing a bulk polymer were calculated in the equilibrated state to quantify how widely the constituents are distributed about the center of mass of the molecule with small radius of gyration corresponding to a collapsed molecule. The radius of gyration is defined as

$$R_g{}^2 = \frac{1}{M} \sum_{i=1}^{N} m_i (\mathbf{r}_i - \mathbf{r}_{COM})^2 \tag{1}$$

where N is the total number of beads of a molecule, $\mathbf{r}_i$ the position of bead i, $\mathbf{r}_{COM}$ the position of the center of mass of the molecule, m_i the mass of bead i, and M the total mass.

Primitive paths were extracted to estimate the extent of chain entanglement in a bulk polymer at an equilibrated state. Primitive paths are defined as paths of the polymer chains obtained by performing reduction of the original chain network.[21−23] This reduction consists of simultaneously contracting all chains to the shortest possible length under the restriction of fixed chain ends and no chains crossing during the reduction. The chain reduction yields physical obstructions since polymer chains are not capable of crossing through other chains. The physical obstructions are expected instantaneous entanglements. We adopted the annealing method to extract a primitive path network.[23,24] We fixed chains ends in space and disabled the intrachain excluded volume interactions while retaining the interchain excluded volume interactions and then ran a simulation at low temperature (0.05 K). We chose this method for extracting the primitive path network over the common approach of geometrically reducing the original chain network to achieve the minimum contour length[25,26] to maintain intrachain cross-links during the chain reduction. Primitive path networks extracted by the annealing method were characterized by the number of monomers between entanglements, N_e, defined as

$$N_e = N \frac{\langle R^2 \rangle}{\langle L_{pp} \rangle^2} \tag{2}$$

where N is the number of bonds, R is the end-to-end distance of a polymer chain, and L_{pp} is the contour length of a primitive path (see Figure S1 for measuring L_{pp} of a primitive path of SCPN).

The bulk density at 150 K was calculated by dividing the total mass of each bulk assembly by the volume of the periodic simulation box.

Segmental dynamics were evaluated by monitoring the evolution of mean-square displacements (MSD) with time of all beads composing all SCPNs. MSD is defined as

$$MSD(t) = \frac{1}{N} \sum_{i=1}^{N} (\mathbf{r}_i(t) - \mathbf{r}_i(0))^2 \tag{3}$$
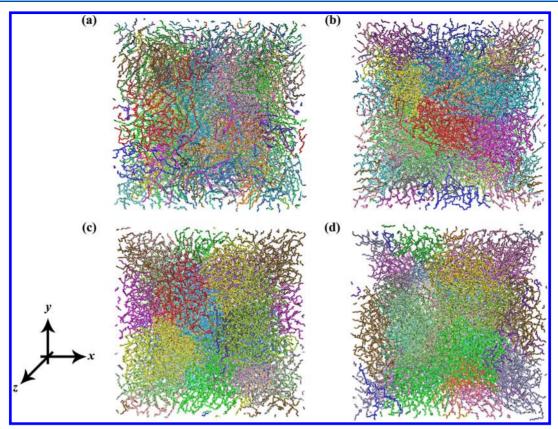
Figure 1. Snapshots of bulk polymer configurations equilibrated at 150 K assembled purely from (a) linear chains and (b−d) SCPNs with 5%, 10%, and 15% cross-linking ratio, respectively. Different colors denote different polymer chains.
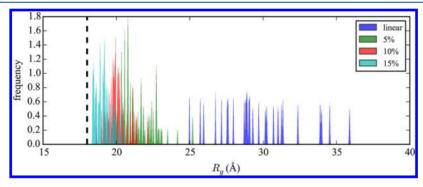

Figure 2. Frequency of radii of gyration of individual molecules (chains/SCPNs) comprising a bulk polymer as a function of cross-linking ratio at 150 K. The dashed line corresponds to the average radii of gyration of individual SCPNs in vacuum. The frequency of radii of gyration for each cross-linking resulted from sampling over three different models.

where N is the total number of beads in an analysis set, $\mathbf{r}_i(t)$ the position of bead i at time t, and $\mathbf{r}_i(0)$ the initial position of bead i. The MSD of all methylene beads were recorded for 100 ns.

2.3. Characterization of Thermomechanical Properties. The prepared models were further analyzed in terms of their thermomechanical properties.

Glass transition temperatures were determined by performing a simulated cooling. To compute this thermal property, we monitored the change in total energy versus temperature while cooling the system from 500 to 10 K at a cooling rate of 0.25 K/ps. It was verified that at this rate the volume change at the rubbery state does not depend on cooling rate (see Figure S3). Two straight lines were fit to the total energy versus temperature data, and the intersection of the straight lines was taken to be the glass transition temperature.[27,28]

The prepared MD models were mechanically tested at 150 K, well into the glassy state for all simulated assemblies. The simulated mechanical testing included displacement controlled uniaxial tension and uniaxial compression. This loading was implemented by deforming the periodic cell along one axis at a constant displacement rate corresponding to an engineering strain rate of $\pm 10^8$ s^{-1}, which is one of strain rates widely used in simulated mechanical testing by means of molecular dynamics simulations. Zero pressure was imposed on the surfaces of the periodic cell along the two lateral axes. We calculated true strain from the ratio of instantaneous length to the initial length of the side of the periodic cell along the applied displacement axis. The response to the deformation was described by true stress along the same axis. True stress was taken from the component of the symmetric pressure tensor known as the virial stress.[29] To take into consideration

different initial SCPN conformations, the stress–strain response for each cross-linking ratio was obtained by averaging results of five different initial configurations. From the stress–strain response we extracted elastic moduli and peak stresses for the different cross-linking ratios.

3. RESULTS AND DISCUSSION

In this section, results are shown for assemblies made from one SCPN model (out of three), unless otherwise stated.

3.1. Configurations at an Equilibrated State. Typical configurations of the SCPN-based bulk polymers equilibrated at 150 K are shown in Figure 1 for each degree of cross-linking. For the assembly of linear chains, chain unfolding is clearly seen and the chains are not easily distinguishable. In contrast, all the SCPN assemblies contain chains that are still folded and relatively independent. To measure to what extent SCPNs are unfolded in the bulk, we extracted the frequency of radii of gyration, R_g, of individual chains in the bulk for assemblies from all three models (Figure 2). Because SCPNs of all cross-linking ratios are made from polymer chains of the same length, a larger radius of gyration indicates a more unfolded chain. For reference, the individual chains in a vacuum, regardless of cross-linking ratio (from 0 to 15%), exhibit a radius of gyration of ∼18 Å. In bulk, linear chains are highly unfolded, exhibiting a broad range in radii of gyration from 25 to 36 Å. SCPNs with 5% cross-linking ratio are less unfolded than the linear chains but still unfolded compared to 10% and 15%. SCPNs with 10% cross-linking ratio are even less unfolded, and SCPNs with 15% cross-linking ratio are the least unfolded with frequency biased to the dashed line (the radius of gyration of chains in vacuum). Interestingly, as the intrachain cross-linking ratio is increased, the radii of gyration of individual SCPNs in a bulk polymer become more like the radii of gyration of an independent SCPN in vacuum. The negligible change in the radii of gyration of the individual SCPNs with 10% and 15% cross-linking ratios implies that SCPNs with 10% and 15% cross-linking ratios are not unfolded in the presence of additional similar particles—individual SCPNs remain compact due to covalent constraints which then limit the ability to create entanglements with surrounding chains. Previous modeling studies have seen a decrease in radius of gyration of SCPNs and linear precursors by moving from dilute to concentrated conditions.[30,31] Interestingly, the behavior here observed is somehow different, likely because the SCPNs were cross-linked in vacuum, which is analogous to a poor solvent. In bulk, we observed a decrease in the radius of gyration of SCPNs with increasing cross-linking ratio since the environment surrounded by similar other chains acts as a good solvent compared to vacuum.

The bulk polymer configurations also differ in terms of density. Figure 3 shows the variation of the density of the assemblies as a function of cross-linking ratio at 150 K. The density increases with an increasing cross-linking ratio from linear to 10% and then drops at 15%. The drop in density at 15% arises from voids created by the movement limitations, as visible in Figure 1d. The large standard deviation for the 15% cross-linking ratio arises from the difference in packing for assemblies from the three different base SCPNs.

A primitive path network extracted from an assembly of polymer chains provides configurational information. A primitive path composed of more interior straight segments means that the corresponding polymer chain is more entangled with other polymer chains. Figure 4 shows the reduced
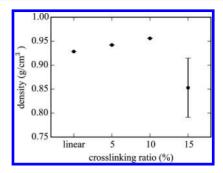

Figure 3. Change in density as a function of intrachain cross-linking ratio. The density for each cross-linking ratio resulted from averages of three different models.

networks of the linear, 5%, 10%, and 15% bulk polymers equilibrated at 150 K. N_e of the reduced network is 204.3 ± 3.5, 421.4 ± 12.5, 999 ± 0, and 999 ± 0, respectively. Recall that the total number of monomers in the chain is 1000. A smaller N_e corresponds to more entanglements. This implies that linear polymer chains physically interact with a greater number of other chains than the SCPNs of all cross-linking ratios in the bulk. The SCPNs with 10% and 15% cross-linking ratios are barely unfolded, restricting only a limited part of the SCPNs to physically interact with other SCPNs. The higher the cross-linking ratio, the less entangled the conformation, which is consistent with our expectation from the snapshots of configurations and the frequency of radii of gyration of individual SCPNs at equilibrium. These findings lead to the conclusion that SCPN architecture limits entanglements between chains; i.e., the effect of intrachain cross-links on interchain interaction is opposite to that of interchain cross-links, which increases the energy of interaction between chains.[32,33]

3.2. Thermomechanical Properties. The calculated glass transition temperatures (T_g) of all the bulk assemblies are shown in Figure 5 as a function of cross-linking ratio. The T_g of the bulk polymers increases with an increasing cross-linking ratio, a trend in agreement with our previous experimental observations.[14] This increase in T_g is attributed to the restriction of molecular dynamics by the presence of covalent constraints. This restriction is analogous to the confinement effect of rigid substrates that strongly interact with polymer films, resulting in the increase in T_g of the films.[34,35] The T_g for all the cross-linking ratios is within the error bar of that calculated by MD for individual SCPNs in a vacuum at the same cooling rate.[17] Because the glass transition temperature ranges only from 220 to 270 K, 150 K was chosen as the reference temperature for investigating the glassy mechanical behavior.

The MD models of the bulk polymers at 150 K were subjected to uniaxial tension and compression by deforming the simulation box at a constant strain rate. Figure 6a shows the stress–strain response to uniaxial tension as a function of cross-linking ratio. The linear bulk polymer shows a stress–strain curve characterized by a linear-elastic regime followed by strain softening and hardening. The slope within the linear-elastic regime, the peak stress, and the failure strain become steeper, larger, and smaller, respectively, from linear to 10%. The 15% assembly shows comparable stiffness to the other polymers but fails at smaller stress and strain. Molecular snapshots of the deformed configurations at a true strain of 0.17 are shown in Figure 7. At this point in strain, the bulk
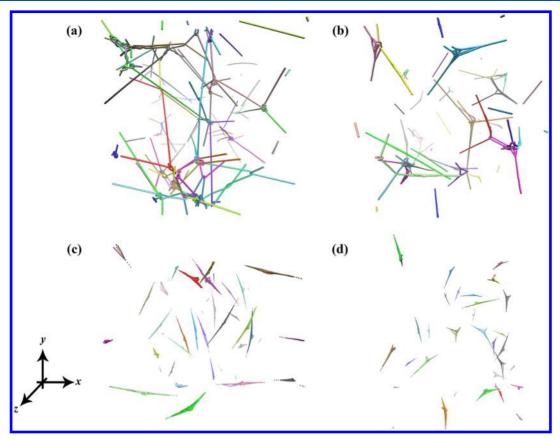
Figure 4. Primitive path network of bulk polymers assembled purely from (a) linear chains and (b–d) SCPNs with 5%, 10%, and 15% cross-linking ratio. Different colors denote different polymer chains.
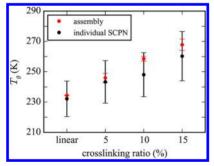

Figure 5. Glass transition temperature (T_g) versus cross-linking ratio. Circular marks stand for mean, and error bars represent the standard deviation. T_g for each cross-linking ratio is the average of three different models.

polymers assembled from linear chains and SCPNs with 5% cross-linking ratio exhibit strain softening, the 10% is about to fail, and the 15% has already failed. It can be seen that the failure is due to separation between SCPNs. The associated mechanical properties are provided in Table 2. We attribute the increase in the stiffness from linear to 10% to the greater number of intrachain cross-links. In the very beginning of deformation, where chain slip governs the deformation behavior,[36] intrachain cross-links likely act equivalently to interchain cross-links to contribute to the increase in the stiffness. At strains beyond yield, the chain topology as tailored by intrachain cross-links starts to dominate. Strain hardening is therefore only observed in the linear bulk polymer in which the distance between entanglements is small. The stress–strain behavior we previously observed experimentally also showed a decrease in ductility with increasing cross-link density but did
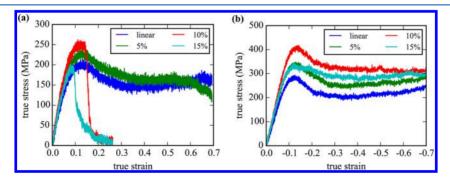

Figure 6. Stress–strain response to (a) uniaxial tension and (b) uniaxial compression of the bulk polymer as a function of cross-linking ratio at a temperature of 150 K and an engineering strain rate of 10^8 s^{-1}.
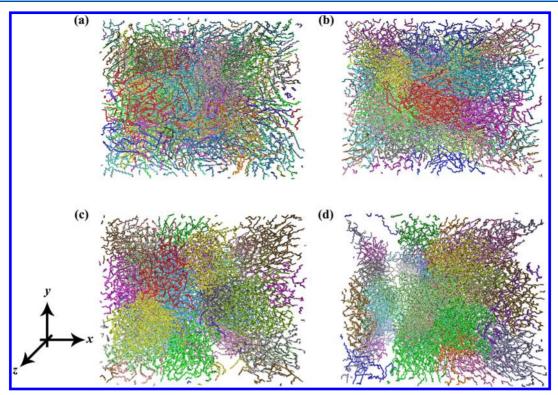
Figure 7. Deformed configuration of bulk polymers assembled purely from (a) linear chains and (b−d) SCPNs with 5%, 10%, and 15% cross-linking ratio at a strain of 0.17. Different colors denote different polymer chains. Deformation is applied in the x-direction.

Table 2. Mechanical Properties as a Function of Cross-Linking Ratio

ratio [%]	elastic modulus[a,b] [GPa]	peak stress[a] [MPa]	peak stress[b] [MPa]
0	3.02 ± 0.52	203.26 ± 8.51	286.78 ± 11.81
5	3.78 ± 0.35	229.19 ± 10.10	339.43 ± 12.30
10	3.93 ± 0.40	252.93 ± 11.24	409.06 ± 13.80
15	3.59 ± 0.52	192.51 ± 13.72	333.34 ± 15.81

[a]Under tension. [b]Under compression.

not show the increase in stiffness and strength. This difference in findings may be due to chemical details, with cross-linking less important for the elastic stiffness of the experimental methyl methacrylate system since the side groups are more substantial or as a consequence of the simulated cross-links being tighter in relation to the ones used in experiments, which were longer and more flexible.

As shown in Figure 6b, all assemblies exhibit an elastic−plastic response under compression with a clear yield peak followed by softening and then mild strain hardening. Compression suppresses the brittle failure mode that was seen under tension. Still, the peak stress increases from linear to 10% and then drops again for 15%. While only the linear bulk polymer exhibits strain hardening under tension, the bulk polymers of all cross-linking ratios do exhibit strain hardening under compression. This hardening is substantially greater for linear and 5% than for the 10% and 15% (see Figure S6 for response at larger strains). As strain hardening is associated with entanglement density in glassy polymers,[1,37−39] this observation is in agreement with the primitive path analysis that shows a lower entanglement density with increasing cross-link ratio. The more entangled conformation of the linear bulk polymer is also likely responsible for the strain hardening under tension while in the 5% assembly there are fewer entanglements (more beads between entanglements), apparently not enough to stabilize the strain softening (Figure 6a).
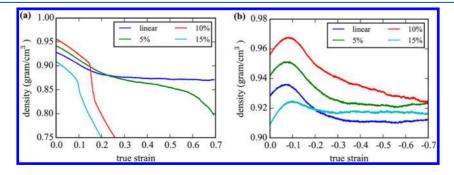

Figure 8. Density change during (a) uniaxial tension and (b) uniaxial compression of the bulk polymer as a function of cross-linking ratio at a temperature of 150 K and an engineering strain rate of 10^8 s^{-1}.
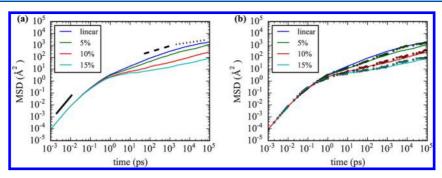
Figure 9. Mean-square displacements at a temperature of 500 K of (a) all beads of the polymers and (b) comparison of free ends and all beads of the bulk polymer assembled from SCPNs as a function of cross-linking ratio. The black solid line, dashed line, and dotted line correspond to MSD $\propto t^2$, $t^{1/2}$, and $t^{1/4}$, respectively. The circles correspond to mean-square displacements of the free ends.
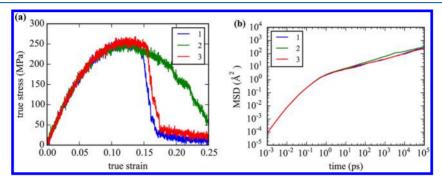

Figure 10. (a) Stress−strain response to uniaxial tension at a temperature of 150 K and an engineering strain rate of 10^8 s^{-1} and (b) mean-square displacements of all beads of the bulk polymers assembled from SCPNs with 10% cross-linking ratio for three different identically processed models (labeled under 1, 2, and 3) at a temperature of 500 K.

Comparing these findings to our previous work on the mechanical properties of individual SCPNs under uniaxial compression, we can observe similar behavior of peak stress increase and then decrease with increasing cross-linking ratio.[17] However, for individual SCPNs, additional cross-linking results in strain hardening, which is not observed in bulk. The reason for that is that an individual SCPN better represents a thermoset, in which all chains are covalently connected, while in the bulk material chains can move relative to each other.

Under tension, for all cross-linking ratios, the system density decreases during elastic deformation. For the linear polymer, the density levels out after strain softening. For the 5% assembly, the density shows a similar change as the density for the linear but decreases with steeper slope again after the stress plateau. For 10% and 15%, the density shows a dramatic drop, corresponding to failure. Under compression, for all cross-linking ratios, the system density increases during elastic deformation and decreases during softening. During the stress plateau, the density keeps decreasing only for 10% and remains constant for the other cross-linking ratios. The density change for the linear polymer is a typical deformation response of a glassy polymer to compression.[40,41] The initial decrease and increase in density for tension and compression respectively are attributable to the elastic Poisson effect. The postyield behavior seems to be a signature of how the SCPN packing changes, with behavior clearly much less driven to decohesion under the positive hydrostatic pressure component of compression as compared to tension.

3.3. Segmental Dynamics. Segmental dynamics of the constituent beads of the SCPNs is one of the keys to understanding the motion of the SCPNs in the bulk polymers, as they strongly influence the assembly configuration and

therefore the thermomechanical properties. Figure 9a shows mean-square displacements (MSD) at 500 K of all beads within all the SCPNs as a function of cross-linking ratio. The MSD of linear chains exhibits first a ballistic regime ($\propto t^2$), a Rouse regime ($\propto t^{1/2}$), and then a one-fourth power law in time starting around 3 ns.[22,42] In this one-fourth power law regime, the linear chains start feeling confining tubes formed by the other polymer chains. At extremely small times ($t < 0.01$ ps), the MSD of the SCPNs falls on top of that of the linear chains regardless of cross-linking ratio. At larger times, however, as the intrachain cross-linking ratio is increased, the MSD evolves at a slower rate because of the intrachain cross-links restricting the motion within the SCPNs. Interestingly, after the ballistic regime the slopes of the SCPNs remain between those characteristic of the Rouse and tube reptation regimes through the 100 ns observed here. The lack of intrachain cross-links allows the polymer chains in the linear model to readily move around and produce a bulk polymer with a configuration shown in Figure 1a with the chains highly unfolded and entangled with each other. In contrast, the SCPNs keep themselves folded with fewer entanglements between them. This finding is also related to the increase in T_g shown in Figure 5, as more thermal energy is required to achieve similar chain mobility as cross-linking ratio increases. Polymer chain penetration and entanglement are also observed in polymer welding, and it is known that chain ends dominate interdiffusion of polymer chains across an interface.[43] Because of the distinct motion of chain ends, we examined the mobility of chain ends of the SCPNs despite them being relatively short. In our study, chain ends are defined as the beads beyond the last cross-link site on each end of each SCPN. Figure 9b shows the MSD of all beads and chain ends in the bulk polymer

assmbled from SCPNs as a function of cross-linking ratio at 500 K. We found that the MSD of chain ends of the SCPNs with 5% cross-linking ratio does exhibit a similar behavior to that of the linear chains at long times. For 10% and 15% cross-linking ratio, in contrast to interfacial welding, the difference in MSD between chain ends and other beads is negligible.

There are moderate differences in the tensile stress–strain behavior of assemblies formed from different SCPN instances with the same cross-linking density, as shown for example for the 10% cross-linking ratio in Figure 10a. Models 1 and 3 fail before a strain of 0.2, and model 2 fails in a more gradual manner, reaching total loss of stiffness at a strain of 0.3. These differences are correlated to differences in the segmental dynamics at 500 K. As shown in Figure 10b, the MSD at 500 K of beads of model 2 are larger than the MSD of models 1 and 3. Model 2 is distinct from models 1 and 3 in terms of the internal structure. Model 2 lacks intrachain cross-links created between beads separated by 100 beads, which makes the beads within each SCPN more mobile relative to each other and failure strain larger than those of models 1 and 3 (see Figure S4b for distance between adjacent cross-link sites for the assembly of SCPNs with 10% cross-linking ratio).

4. CONCLUSION

In this study we created MD models representative of bulk polymers assembled purely from SCPNs and used these models to observe and analyze the thermomechanical behavior as a function of intrachain cross-linking ratio. For all cross-linking ratios (5%, 10%, and 15%), three different MD models were prepared from three different precursory SCPNs and investigated. The prepared bulk polymers were analyzed in terms of their configurations and dynamics at an equilibrated state and mechanically tested in the glassy state.

We observed that the chain topology of a bulk polymer changes with intrachain cross-linking ratio. Molecular snapshots provided insights into the chain topology, where the highly cross-linked SCPNs are readily distinguishable within the bulk, whereas the linear chains are highly unfolded and fully intermixed. The extent of unfolding of SCPNs was quantified by the radii of gyration of individual SCPNs. A primitive path network also provided information about the SCPN assembly microstructure. The extent of interchain entanglement was estimated by the average number of monomers between entanglements, N_e, along the primitive paths. The tightly cross-linked SCPNs physically interact less with each other than linear chains, as indicated by a larger number of N_e. The glass transition temperature increases with higher cross-linking ratio, and this trend is consistent with the decreasing segmental mobility at the annealing temperature as intrachain cross-links are added.[44] The mechanical tests revealed that as the intrachain cross-linking ratio is increased from 0 to 10% the bulk polymers become stiffer and stronger, but more brittle. The 15% assembly behaves distinctly with a reduced stiffness and brittle failure resulting from poor packing. Because entanglements have a critical role in stabilizing strain softening during large deformation, the bulk polymers assembled from SCPNs of all cross-linking ratios show postyield behavior without strain hardening under tension.

Our simulation results indicate that intrachain cross-linking can be used to change the underlying structure of a bulk polymer and therefore the thermomechanical properties. The main role of intrachain cross-links we observed is to restrict the movement of constituent beads of SCPNs and control the chain unfolding and chain entanglement even when SCPNs are surrounded by other SCPNs. Our findings from this MD study support our hypothesis from experiments that there is less potential for interchain entanglements with increasing intrachain cross-linking ratio.[14] Here we varied only the amount of intrachain cross-links, but there are numerous other design variables such as cross-link functionality, cross-link length, and cross-linking site distribution along the initial linear chains in addition to different types of noncovalent interactions between chains, all of which can affect the final material properties. Regardless of the design variables, the chain motion scales with the temperature and the thermomechanical behavior above the glass transition temperature is expected to differ from that below the glass transition temperature. Future work will focus on investigation of chain entanglement between SCPNs in the bulk and its effect on the thermomechanical properties above the glass transition temperature.

■ ASSOCIATED CONTENT

⑤ Supporting Information

The Supporting Information is available free of charge on the ACS Publications website at DOI: 10.1021/acs.macromol.8b01027.

> Figures S1–S9: details on estimation of the length of primitive paths, stress–strain response curve convergence, glass transition temperature comparison, and stress–strain response and mean-square displacements for three different identically processed models (PDF)

■ AUTHOR INFORMATION

Corresponding Author

*(M.N.S.) E-mail meredith.silberstein@cornell.edu, Ph +1 607-255-5063.

ORCID ⦿

Suwon Bae: 0000-0002-9263-5817
Charles E. Diesendruck: 0000-0001-5576-1366

Notes

The authors declare no competing financial interest.

■ ACKNOWLEDGMENTS

■ REFERENCES

(1) Van Melick, H. G.; Govaert, L. E.; Meijer, H. E. On the origin of strain hardening in glassy polymers. *Polymer* **2003**, *44*, 2493–2502.

(2) Myung, D.; Koh, W.; Ko, J.; Hu, Y.; Carrasco, M.; Noolandi, J.; Ta, C. N.; Frank, C. W. Biomimetic strain hardening in interpenetrating polymer network hydrogels. *Polymer* **2007**, *48*, 5376–5387.

(3) Kingsbury, C. M.; May, P. A.; Davis, D. A.; White, S. R.; Moore, S.; Sottos, N. R. Shear activation of mechanophore-crosslinked polymers. *J. Mater. Chem.* **2011**, *21*, 8381.

(4) Li, C.-H.; Wang, C.; Keplinger, C.; Zuo, J.-L.; Jin, L.; Sun, Y.; Zheng, P.; Cao, Y.; Lissel, F.; Linder, C.; You, X.-Z.; Bao, Z. A highly stretchable autonomous self-healing elastomer. *Nat. Chem.* **2016**, *8*, 618–624.

(5) Vidavsky, Y.; Bae, S.; Silberstein, M. Modulating metallopolymer mechanical properties by controlling metal ligand crosslinking. *J. Polym. Sci., Part A: Polym. Chem.* **2018**, *56*, 1117.

(6) Bačová, P.; Lo Verso, F.; Arbe, A.; Colmenero, J.; Pomposo, J. A.; Moreno, A. J. The Role of the Topological Constraints in the Chain Dynamics in All-Polymer Nanocomposites. *Macromolecules* **2017**, *50*, 1719−1731.

(7) Ouchi, M.; Badi, N.; Lutz, J.-F. J.; Sawamoto, M. Single-chain technology using discrete synthetic macromolecules. *Nat. Chem.* **2011**, *3*, 917−24.

(8) Mecerreyes, D.; Lee, V.; Hawker, C. J.; Hedrick, J. L.; Wursch, A.; Volksen, W.; Magbitang, T.; Huang, E.; Miller, R. D. A Novel Approach to Functionalized Nanoparticles: Self-Crosslinking of Macromolecules in Ultradilute Solution. *Adv. Mater.* **2001**, *13*, 204−208.

(9) Aiertza, M. K.; Odriozola, I.; Cabañero, G.; Grande, H.-J.; Loinaz, I. Single-chain polymer nanoparticles. *Cell. Mol. Life Sci.* **2012**, *69*, 337−46.

(10) Harth, E.; Van Horn, B.; Lee, V. Y.; Germack, D. S.; Gonzales, C. P.; Miller, R. D.; Hawker, C. J. A facile approach to architecturally defined nanoparticles via intramolecular chain collapse. *J. Am. Chem. Soc.* **2002**, *124*, 8653−8660.

(11) Murray, B. S.; Fulton, D. A. Dynamic covalent single-chain polymer nanoparticles. *Macromolecules* **2011**, *44*, 7242−7252.

(12) Altintas, O.; Barner-Kowollik, C. Single chain folding of synthetic polymers by covalent and non-covalent interactions: Current status and future perspectives. *Macromol. Rapid Commun.* **2012**, *33*, 958−971.

(13) Stals, P. J. M.; Gillissen, M. A. J.; Nicolaÿ, R.; Palmans, A. R. A.; Meijer, E. W. The balance between intramolecular hydrogen bonding, polymer solubility and rigidity in single-chain polymeric nanoparticles. *Polym. Chem.* **2013**, *4*, 2584.

(14) Galant, O.; Bae, S.; Wang, F.; Levy, A.; Silberstein, M. N.; Diesendruck, C. E. Mechanical and Thermomechanical Characterization of Glassy Thermoplastics with Intrachain Cross-Links. *Macromolecules* **2017**, *50*, 6415−6420.

(15) Mayo, S. L.; Olafson, B. D.; Goddard, W. A. DREIDING: a generic force field for molecular simulations. *J. Phys. Chem.* **1990**, *94*, 8897−8909.

(16) Hossain, D.; Tschopp, M.; Ward, D.; Bouvard, J.; Wang, P.; Horstemeyer, M. Molecular dynamics simulations of deformation mechanisms of amorphous polyethylene. *Polymer* **2010**, *51*, 6071−6083.

(17) Bae, S.; Galant, O.; Diesendruck, C. E.; Silberstein, M. N. Tailoring single chain polymer nanoparticle thermomechanical behavior by cross-link density. *Soft Matter* **2017**, *13*, 2808−2816.

(18) Plimpton, S. Fast Parallel Algorithms for Short-Range Molecular Dynamics. *J. Comput. Phys.* **1995**, *117*, 1−19.

(19) Towns, J.; Cockerill, T.; Dahan, M.; Foster, I.; Gaither, K.; Grimshaw, A.; Hazlewood, V.; Lathrop, S.; Lifka, D.; Peterson, G. D.; Roskies, R.; Scott, J. R.; Wilkens-Diehr, N. XSEDE: Accelerating Scientific Discovery. *Comput. Sci. Eng.* **2014**, *16*, 62−74.

(20) Humphrey, W.; Dalke, A.; Schulten, K. VMD − Visual Molecular Dynamics. *J. Mol. Graphics* **1996**, *14*, 33−38.

(21) Edwards, S. F. The theory of rubber elasticity. *Br. Polym. J.* **1977**, *9*, 140−143.

(22) Rubinstein, M.; Colby, R. H. *Polymer Physics*; Oxford University Press: 2003; p 374.

(23) Everaers, R.; Sukumaran, S. K.; Grest, G. S.; Svaneborg, C.; Sivasubramanian, A.; Kremer, K. Rheology and Microscopic Topology of Entangled Polymeric Liquids. *Science* **2004**, *303*, 823−826.

(24) Sukumaran, S. K.; Grest, G. S.; Kremer, K.; Everaers, R. Identifying the primitive path mesh in entangled polymer liquids. *J. Polym. Sci., Part B: Polym. Phys.* **2005**, *43*, 917−933.

(25) Kröger, M. Shortest multiple disconnected path for the analysis of entanglements in two- and three-dimensional polymeric systems. *Comput. Phys. Commun.* **2005**, *168*, 209−232.

(26) Foteinopoulou, K.; Karayiannis, N. C.; Mavrantzas, V. G.; Kröger, M. Primitive path identification and entanglement statistics in polymer melts: Results from direct topological analysis on atomistic polyethylene models. *Macromolecules* **2006**, *39*, 4207−4216.

(27) Fukui, K.; Sumpter, B. G.; Barnes, M. D.; Noid, D. W. Atomistic Dynamics of Nanoscale Polymer Particles. *Macromolecules* **2000**, *33*, 5982−5987.

(28) Merling, W. L.; Mileski, J. B.; Douglas, J. F.; Simmons, D. S. The Glass Transition of a Single Macromolecule. *Macromolecules* **2016**, *49*, 7597−7604.

(29) Thompson, A. P.; Plimpton, S. J.; Mattson, W. General formulation of pressure and stress tensor for arbitrary many-body interaction potentials under periodic boundary conditions. *J. Chem. Phys.* **2009**, *131*, 154107.

(30) Moreno, A. J.; Lo Verso, F.; Arbe, A.; Pomposo, J. A.; Colmenero, J. Concentrated Solutions of Single-Chain Nanoparticles: A Simple Model for Intrinsically Disordered Proteins under Crowding Conditions. *J. Phys. Chem. Lett.* **2016**, *7*, 838−844.

(31) González-Burgos, M.; Arbe, A.; Moreno, A. J.; Pomposo, J. A.; Radulescu, A.; Colmenero, J. Crowding the Environment of Single-Chain Nanoparticles: A Combined Study by SANS and Simulations. *Macromolecules* **2018**, *51*, 1573−1585.

(32) Davidson, J. D.; Goulbourne, N. C. Nonaffine chain and primitive path deformation in crosslinked polymers. *Modell. Simul. Mater. Sci. Eng.* **2016**, *24*, 065002.

(33) Galant, O.; Davidovich-Pinhas, M.; Diesendruck, C. E. The Effect of Intramolecular Cross-Linking on Polymer Interactions in Solution. *Macromol. Rapid Commun.* **2018**, *39*, 1800407.

(34) Hudzinskyy, D.; Lyulin, A. V.; Baljon, A. R. C.; Balabaev, N. K.; Michels, M. A. J. Effects of strong confinement on the glass-transition temperature in simulated atactic polystyrene films. *Macromolecules* **2011**, *44*, 2299−2310.

(35) Xu, J.; Ding, L.; Chen, J.; Gao, S.; Li, L.; Zhou, D.; Li, X.; Xue, G. Sensitive characterization of the influence of substrate interfaces on supported thin films. *Macromolecules* **2014**, *47*, 6365−6372.

(36) Edwards, S.; Vilgis, T. The effect of entanglements in rubber elasticity. *Polymer* **1986**, *27*, 483−492.

(37) Donald, A. M.; Kramer, E. J. Effect of molecular entanglements on craze microstructure in glassy polymers. *J. Polym. Sci., Polym. Phys. Ed.* **1982**, *20*, 899−909.

(38) Tervoort, T. A.; Govaert, L. E. Strain-hardening behavior of polycarbonate in the glassy state. *J. Rheol.* **2000**, *44*, 1263−1277.

(39) Hoy, R. S.; Robbins, M. O. Strain hardening in polymer glasses: Limitations of network models. *Phys. Rev. Lett.* **2007**, *99*, 1−4.

(40) Capaldi, F. M.; Boyce, M. C.; Rutledge, G. C. Enhanced Mobility Accompanies the Active Deformation of a Glassy Amorphous Polymer. *Phys. Rev. Lett.* **2002**, *89*, 175505.

(41) Capaldi, F. M.; Boyce, M. C.; Rutledge, G. C. Molecular response of a glassy polymer to active deformation. *Polymer* **2004**, *45*, 1391−1399.

(42) Doi, M.; Edwards, S. F. *The Theory of Polymer Dynamics*; Clarendon Press: Oxford, 1986; p 374.

(43) Ge, T.; Pierce, F.; Perahia, D.; Grest, G. S.; Robbins, M. O. Molecular dynamics simulations of polymer welding: Strength from interfacial entanglements. *Phys. Rev. Lett.* **2013**, *110*, 1−5.

(44) Tsige, M.; Taylor, P. L. Simulation study of the glass transition temperature in poly(methyl methacrylate). *Phys. Rev. E: Stat. Phys., Plasmas, Fluids, Relat. Interdiscip. Top.* **2002**, *65*, 021805.